Journal of Directed Energy, **2**, Spring 2007, 211–223

Estimates of Atmospheric Distortion Number for Nonlinear Refraction

J. R. Roadcap*

Institute for Scientific Research, Boston College, Chestnut Hill, Massachusetts 02467, and Space Vehicles Directorate, Air Force Research Laboratory, Hanscom Air Force Base, Massachusetts 01731

and

P. J. McNicholl, R. R. Beland, and G. Y. Jumper

Space Vehicles Directorate, Air Force Research Laboratory, Hanscom Air Force Base, Massachusetts 01731

A characteristic nondimensional distortion number N_d was derived in the 1970s that allows inference of the degree of nonlinear refraction or thermal blooming associated with an atmospheric laser path. For a continuous-wave (CW) laser with a Gaussian-shaped beam, the distortion number is a function of several variables including laser power and aperture size, optical wavelength, atmospheric absorption and extinction, index of refraction, temperature, air density, and the air speed or flow transverse to the laser beam. Scenario-dependent calculations of atmospheric distortion number N_d are developed for different geographic regions and seasons using the Air Force Research Laboratory's global thermosonde database, the HITRAN molecular spectroscopic database, and global climatological aerosol model extinction profiles. Tactical air-to-ground scenarios are described as a function of altitude, target distance, and laser-to-target azimuth angle for the COIL wavelength (1.315 μm). The results are interpreted in light of seasonal and geographical factors as well as path-integrated moisture.

KEYWORDS: Distortion number, Molecular absorption, Refraction, Thermal blooming

Nomenclature

a	laser aperture radius, m
C_T^2	turbulent temperature structure constant, $K^2\ m^{-2/3}$
c_p	specific heat of air at constant pressure, $J\ kg^{-1}\ K^{-1}$
$I_b\ I_0$	area-averaged intensities at focal plane center for blooming, diffraction-limited propagation, respectively, $W\ m^{-2}$
I_p	normalized peak irradiance
k	laser wave number, m^{-1}
N_A	absorption number
N_d	distortion number

Received February 18, 2006; revision received November 1, 2006.
*Corresponding author; e-mail: John.Roadcap@hanscom.af.mil.

N_F	Fresnel number
N_w	slew number
n	index of refraction of air at laser wavelength
P	laser power, J s^{-1}
r_m	laser beam radius, m
S	atmospheric path range or total distance, m
SPW	slant path precipitable water, cm
s	distance along laser path from source to receiver, m
T	virtual air temperature, K
w	water vapor mixing ratio, g kg^{-1}
z_0	nonlinear interaction parameter, m
α_t	atmospheric total absorption coefficient, m^{-1}
ε	index of refraction perturbation
λ	laser wavelength, μm
v_n	beam transverse air speed, m s^{-1}
ρ	air density, kg m^{-3}
ρ_d	density of dry air, kg m^{-3}
ρ_l	density of liquid water, kg m^{-3}
σ	atmospheric extinction, m^{-1}

1. Introduction

Nonlinear refraction, often referred to as "thermal blooming," is the distortion of the laser irradiance field caused by its interaction with the mean index of refraction field of the atmosphere. The effects of thermal blooming are related to the local heating of the atmosphere caused by the absorption of the high-energy laser (HEL) energy and the advection of heat by beam-transverse flow as the laser wave front propagates through the atmosphere. This interaction between the laser power and the atmosphere is nonlinear. Thermal blooming effects can be numerically computed by integrating the paraxial wave equation approximation to Maxwell's equation (e.g., Refs. 7 and 17). This equation includes a simplified steady-state relation between refractive and irradiance fields that is derived from the linearized equations of hydrodynamics.

Wallace and Camac[16] derived a nonlinear interaction parameter or distance z_0. They described z_0 as the propagation distance at which the nonlinear refraction effects caused by transverse density gradients distributed over the laser beam width will distort the irradiance distribution significantly. For a continuous-wave (CW) laser, z_0 is expressed as the ratio of the laser beam radius r_m to the square root of the normalized index of refraction perturbation ε:

$$\varepsilon = \frac{(n-1)\alpha_t P}{\pi \rho c_p T v_n r_m}, \tag{1}$$

where n is the refractive index of air at the laser wavelength, α_t is the atmospheric total absorption coefficient at the laser wavelength, P is laser power, ρ is air density, c_p is the specific heat of air at constant pressure, T is the virtual air temperature, and v_n is the beam normal or transverse air speed. The virtual air temperature, which satisfies the equation of state for dry air in a moist atmosphere, is a function of air temperature and water vapor mixing ratio. The form of Eq. (1) implies a homogeneous atmosphere. The transverse air speed v_n is assumed to be subsonic.

Bradley and Herrmann[2] defined a similar expression, calling it the nondimensional distortion number N_d, and used it to quantify the degree of thermal blooming associated with an atmospheric path range or focal length S. Gebhardt[5] generalized their expression for a nonhomogeneous path [see Eqs. (4.22) and (4.24) in Ref. 5]. For a CW laser, this is expressed as

$$N_d = -\frac{P_t \cdot k}{a} \int_0^S \frac{\alpha(s) e^{-\int_0^s \sigma(s)\mathrm{d}s} \mathrm{d}n/\mathrm{d}T}{c_p n(s) \rho(s) v_n(s)} \mathrm{d}s, \tag{2}$$

where the variable symbols are the same as described in Eq. (1). Here P_t is the laser power at the laser aperture of radius a, k is the laser wave number, σ is the atmospheric extinction, and s is the distance along the laser path from source to receiver.

2. Relation of N_d to Laser Beam Distortion

The relation of N_d to laser beam irradiance field distortion due to nonlinear refraction is illustrated by integrating the paraxial wave equation of Bradley and Herrmann [Ref. 2, Eq. (3)] in the propagation direction for a CW laser with circular aperture. This nondimensional differential equation includes both the atmospheric distortion number and a set of three other nondimensional numbers including the Fresnel number N_F, absorption number N_a, and slew number N_w. We integrated this equation using the alternate-direction implicit finite element method (Ref. 4, Chapter 4). Figure 1a depicts an image of normalized irradiance on the focal plane for diffraction-limited effects, i.e., accounting for no atmosphere. Figure 1b shows the irradiance field for steady-state uncompensated propagation of the CW

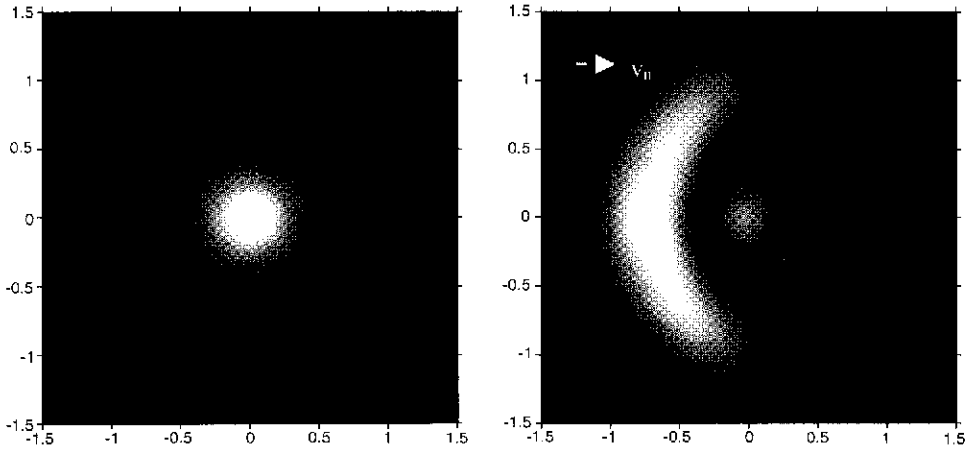

a) Diffraction limited (no atmosphere)

b) Uncompensated thermal blooming

Fig. 1. Simulated images of the focal plane irradiance depicting a) diffraction limited and b) uncompensated blooming occurring with steady-state CW HEL Gaussian beam propagation in a homogeneous atmosphere. The propagation direction is normal to the page, and the beam-transverse flow is from left to right in panel b. The transverse coordinates are scaled by beam radius. Irradiance levels are proportional to shade lightness.

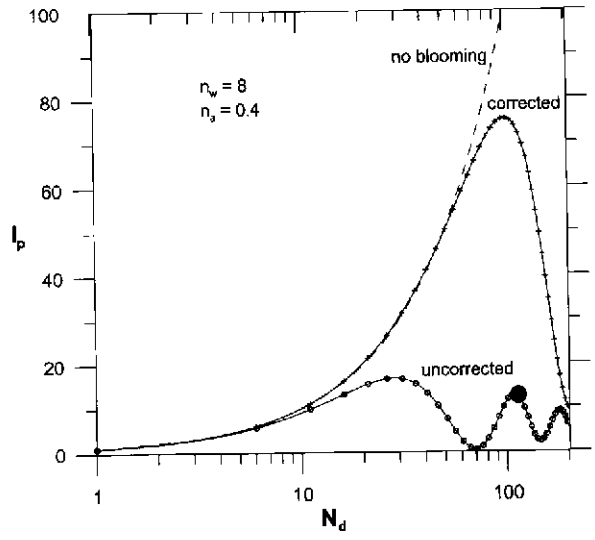

Fig. 2. Normalized peak intensity I_p as a function of atmospheric distortion number N_d. Even with phase compensation, significant intensity reduction begins for $N_d > 100$. The black circle corresponds to N_d for the uncompensated blooming depicted in Fig. 1b. The slew number N_w and absorption number N_a are also shown in the diagram of Bradley and Herrmann.[2]

laser through a homogeneous atmosphere where the distortion number N_d exceeds 100. Effects of refractive turbulence on the laser irradiance field are not included. The transverse flow speed v_n is directed from left to right in the figure. In the presence of an atmosphere and thermal blooming (Fig. 1b), significant phase and amplitude distortions of the laser irradiance occur.

Figure 2 depicts the change of the normalized peak irradiance I_p as a function of distortion number N_d for uncompensated and phase-compensated atmospheric effects. Here, I_p is defined as

$$I_p = N_d \frac{I_b}{I_0}, \tag{3}$$

where I_b and I_0 are the area-averaged intensities near the center of the focal plane for thermal blooming and diffraction-limited propagation, respectively. The ratio I_b/I_0 is similar to the Strehl intensity defined in Born and Wolf [Ref. 1, Chapter 9, Eq. (9)]. Increasing N_d while holding the atmospheric parameters fixed is equivalent to increasing the laser aperture power. In the case of uncorrected blooming, the normalized peak irradiance I_p begins to decrease at relatively small values of $N_d \sim 30$. Phase-compensated propagation, using Eq. (4) of Bradley and Herrmann,[2] permits the normalized peak irradiance to increase for values of $N_d \leq 100$, after which I_p drops rapidly once the distortion number exceeds a critical value. Thus, increasing the distortion number, whether through a power increase or atmospheric absorption increase, can eventually lead to decreased intensity in the focal plane, even when the beam is phase compensated near the aperture.

3. Estimating the Atmospheric Distortion Number N_d

The data source for the atmospheric distortion number analyses are thermosonde vertical profile measurements. Thermosondes are balloon-borne payloads that measure in situ the turbulent temperature structure constant C_T^2 approximately every 7–8 m in the vertical using fine-wire probes. C_T^2 measurements and the associated refractive turbulence are not included in the distortion number calculations here. In addition to C_T^2, the thermosondes measure pressure, temperature, humidity, and horizontal wind velocity using attached radiosondes. In practice, synoptic radiosonde data could be substituted for thermosonde data in these estimates, but this would result in significantly lower vertical resolution.

Equation (2) is evaluated by integrating along an air-to-ground slant path (nonrefracted ray) assuming a spherical earth. For the slant path, the upper end is defined in terms of altitude above mean sea level (MSL), the lower or ground end is set at 5 m above the surface, and the path length is defined in terms of earth surface distance. The calculations are performed for a range of altitudes—up to 6 km above MSL—and for earth surface distances—5–35 km—which bound approximate tactical scenarios. These altitudes and surface distances approximate a range of tactical scenarios.

The evaluation of the beam transverse wind speed v_n along the path includes both the beam slew velocity and horizontal wind velocity measured by the thermosonde. The slew speed path component is evaluated using an upper-end air speed of 100 m/s with 360-deg heading, a fixed (stationary) point at the ground, and three different target azimuths (0, 45, and 90 deg) relative to the upper-end heading. The laser aperture radius is set at 50 cm, and the laser power is 10^5 W (Ref. 5, Table 4.2). The wavelength of 1.315 μm used for the Chemical Oxygen-Iodine Laser (COIL)[12] is selected. Table 1 lists the fixed parameters used in the evaluation of Eq. (2). The air density ρ, refractive index n, and temperature T along the path are determined from the thermosonde measurements.

The atmospheric absorption α and extinction σ at the laser wavelength are important factors in determining the distortion number for tactical scenarios. However, their determination is not as straightforward as for the other variables. In this study, the absorption coefficient represents the sum of molecular line-by-line absorption, continuum absorption, and aerosol absorption, which should be treated differently from molecular absorption for thermal blooming, as described below. The extinction coefficient is the sum of

Table 1. Fixed parameters for calculation of the atmospheric distortion number N_d using Eq. (2)

Fixed parameter type	Magnitude
Laser beam diameter	1 m
Laser wavelength	1.315 μm
Laser power	10^5 W
Upper-end air speed	100 m/s
Lower-end ground speed	0 m/s
Lower-end altitude	5 m AGL
Upper-end altitudes	0.5–6 km MSL
Upper-end heading	360 deg
Lower-end azimuth angles	0, 45, 90 deg

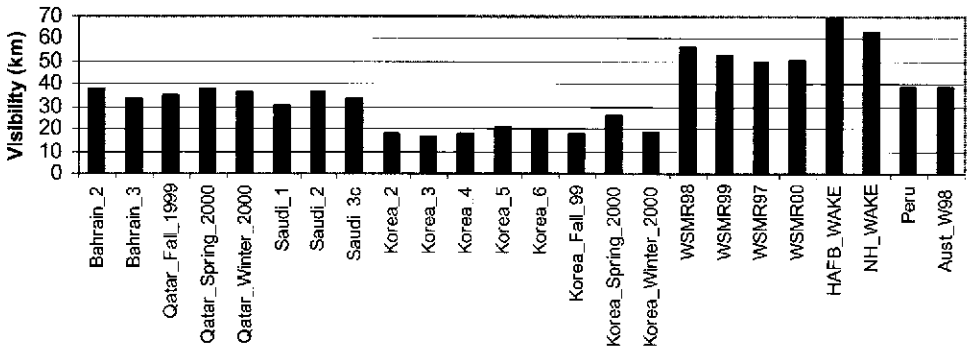

Fig. 3. Average surface visibilities (meteorological range) at different locations and during different seasons for thermosonde measurement campaigns based on the GADS aerosol data sets.

total absorption, molecular scattering, and aerosol scattering. The molecular absorption at 1.315 μm is determined from line-by-line calculations using the HITRAN molecular database,[13] including the molecular continua, and the thermosonde-measured vertical profiles of temperature, pressure, and relative humidity. The aerosol extinction and absorption parameters are derived using thermosonde data and the Optical Properties of Aerosols and Clouds (OPAC)/Global Aerosol Data Sets (GADS).[8,10] GADS provides a climatological database of aerosol absorption and extinction profiles for a 5×5 deg global grid given geographical location, season (summer or winter), and surface relative humidity. One of seven possible aerosol altitude profile types is assigned to each grid point The global model, in principle, distinguishes on a finer scale the aerosol mixtures over various regions. The aerosol extinction at 1.315 μm is based on an objectively determined surface visibility or meteorological range at 0.55 μm provided by the GADS model data, the aerosol model's relative extinction (i.e., extinction at 1.315 μm relative to 0.55 μm), and the particular aerosol model's vertical profile of relative extinction. The visibility or meteorological range (MR) is related to the extinction at 0.55 μm by the relation[9]

$$\mathrm{MR} \simeq 3.0/\sigma \qquad (\mathrm{km}), \tag{4}$$

where σ is the surface extinction coefficient at 0.55 μm. Figure 3 shows the average campaign visibilities for several locations and seasons as determined from GADS climatology.

Figure 3 illustrates the considerable variation between regions in climatological surface visibilities. Here Korea exhibits the lowest visibilities (largest visible extinction) while locations in the United States, on average, experience the highest visibilities.

Figure 4 displays a typical vertical profile of total absorption and extinction based on the combination of HITRAN and the GADS model using input from a thermosonde measurement at Holloman Air Force Base, New Mexico, which is adjacent to the White Sands Missile Range (WSMR). Note that the surface elevation is approximately 1.3 km above MSL. The principal variable molecular constituent influencing absorption is water vapor or humidity. Near the surface, the molecular line absorption at 1.315 μm is typically dominated by water vapor. Every significant feature can be associated with a water vapor transition. Up to around 2 km above ground level (AGL), near the top of the atmospheric boundary layer, the aerosol scattering magnitude dominates molecular absorption. Above the atmospheric boundary layer, line-by-line absorption is the dominant contribution to both absorption and extinction. Of the two parameters, molecular and aerosol optical depth, the aerosol

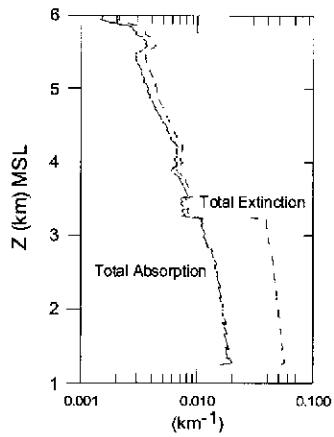

Fig. 4. Vertical profiles of total absorption and extinction at 1.315 μm computed using the HITRAN molecular absorption and GADS aerosol databases. These profiles were computed using data from a thermosonde profile at Holloman Air Force Base, New Mexico, on 6 June 1999 at 0208 MDT. The influence of the boundary-layer aerosol in the extinction curve and, to a much lesser extent, in the absorption curve is evident below 2 km AGL.

component is subject to more uncertainty due to its reliance on climatological means and the inability to directly infer its vertical distribution.

Aerosol absorption (and conduction) contributions are also dependent on the HEL intensity magnitude[15] and aerosol vaporization. As discussed in detail by Sprangle et al.,[14] the aerosol absorption contribution to thermal blooming for hygroscopic aerosols should be normalized by the term $(1 + \eta)$, where η is a constant of order unity representing the ratio of laser energy going into vaporization to laser energy conducted into the air. The ratio η is not accounted for in this paper. The aerosol absorption coefficient is not decreased significantly by the presence of nonhygroscopic aerosols. For a moist humid lower boundary layer, such as found near the Persian Gulf or in southern New Mexico during summer, the aerosol absorption contribution can be much less than 10% of total absorption at 1.315 μm. For a dry boundary layer, such as in Korea in winter, the aerosol absorption contribution at 1.315 μm can exceed 50%. Above the atmospheric boundary layer, the aerosol contribution to total absorption is typically less than 10%. Prevailing meteorological conditions, location, and season determine the relative molecular and aerosol absorption contribution as a function of altitude.

4. Data Sets Analysis with Example

Twenty-one thermosonde data sets from different geographical locations and seasons were used in the analyses. Their location, season, and number of usable profiles for distortion number N_d calculations are listed in Table 2. These sets or "campaigns," each consisting initially of approximately 20–30 vertical profiles, are used to calculate the vertical profiles of molecular and aerosol absorption and scattering from the temperature, pressure, and humidity profile data, as well as to determine the path-normal transverse flow speed using the wind velocity measurements. After all atmospheric variables in a vertical profile are screened and determined to be suitable for analysis, the profiles are individually analyzed for up to 84 slant paths (7 surface distances at 5-km increments for 12 upper-end altitudes

Table 2. Summary of range and mean values for atmospheric distortion number N_d by thermosonde campaign[a]

Year	No. of files	Location	Season	N_d (360 deg)	Mean	N_d (45 deg)	Mean	N_d (90 deg)	Mean
1997	16	Bahrain	Spring	<20–200+	78.4	<10–25+	21.9	<10–20+	14.6
1997	26	Bahrain	Summer	<20–150+	69.2	<15–30+	22.3	<10–20+	15.3
1997	18	Riyadh, SA	Fall	<20–300+	92.1	<10–40+	24.2	<10–25+	14.9
1999	11	Riyadh, SA	Winter	<10–150+	41.1	<5–15+	12.5	<5–15+	10.6
1998	6	Riyadh, SA	Spring	<10–150+	57.6	<10–20+	14.9	<5–15+	9.8
1997	15	Korea	Spring	<20–200+	57.8	<15–40+	24.9	<10–35+	18.3
1997	11	Korea	Summer	<30–200+	89.6	<10–40+	28.1	**<10–40+**	19.1
1997	14	Korea	Fall	<20–200+	66.6	<10–40+	22.4	<10–30+	15.3
1998	23	Korea	Winter	<10–100+	37.7	<5–20+	14.4	<5–15+	9.8
1998	13	Korea	Spring	<20–200+	87.7	<10–40+	21.6	<10–30+	16.4
1998	19	Australia	Winter	<10–200+	52.9	<5–25+	18.1	<5–25+	15.1
1998	13	Peru	Winter	<20–200+	96.9	**<15–50+**	31.6	**<10–40+**	**25.5**
1999	19	Korea	Fall	<10–150+	54.6	<10–25+	15.4	<5–20+	11.1
2000	18	Korea	Winter	***<10–80+***	***21.6***	<5–15+	***6.8***	<5–10+	***5.7***
2000	16	Korea	Spring	<20–300+	79.9	<10–40+	22.9	<10–30+	19.8
1999	19	Qatar	Fall	<20–200+	56.2	<10–25+	19.1	<10–15+	13.8
2000	7	Qatar	Winter	<10–150+	35.5	<5–10+	8.1	<5–10+	8.1
2000	7	Qatar	Spring	<10–150+	39.3	***<5–5+***	***6.8***	***<5–5+***	5.9
1997	10	Holloman	Fall	**<30–400+**	**194.8**	**<15–50+**	**27.5**	**<10–40+**	19.5
1998	9	Holloman	Spring	<10–200+	43.8	<5–15+	12.0	<5–15+	10.2
1999	20	Holloman	Summer	<20–400+	85.9	<10–35+	23.6	<5–15+	18.9

[a]In each column, the largest and smallest values of distortion number are highlighted in boldface. SA, Saudi Arabia.

at 500-m vertical increments). Using a campaign set, the means were computed for each individual slant path for each campaign and plotted.

The most frequent reason for rejection of a campaign data profile was missing wind data. For "head-on" (360 deg) targets, the availability of usable wind data was especially important for slant paths that extended relatively long distances at low altitudes. Three of the campaigns depicted in Fig. 3 (WSMR00, HAFB_WAKE, and NH_WAKE) were not used for distortion number calculations because of lack of good wind data or insufficient number of usable wind profiles. In all, 310 thermosonde profiles were found to be suitable to be analyzed for the 21 campaign data sets. A total of 24,570 separate slant paths were drawn for the analysis.

Figure 5 depicts the pattern of mean distortion number N_d for the Bahrain summer 1997 campaign as a function of laser altitude above MSL and earth surface range for two different aspect angles, 360 and 45 deg, for a focused laser beam. A total of 16 thermosonde profiles were analyzed to produce these plots. In the upper figure (360-deg azimuth), the surface target lies in the direction of the aircraft heading, and the beam transverse flow due to air speed thus is minimal. As a result, N_d values exceeding 100, a critical value for the laser with phase compensation according to Fig. 2, appear for altitudes below 1.5 km MSL and

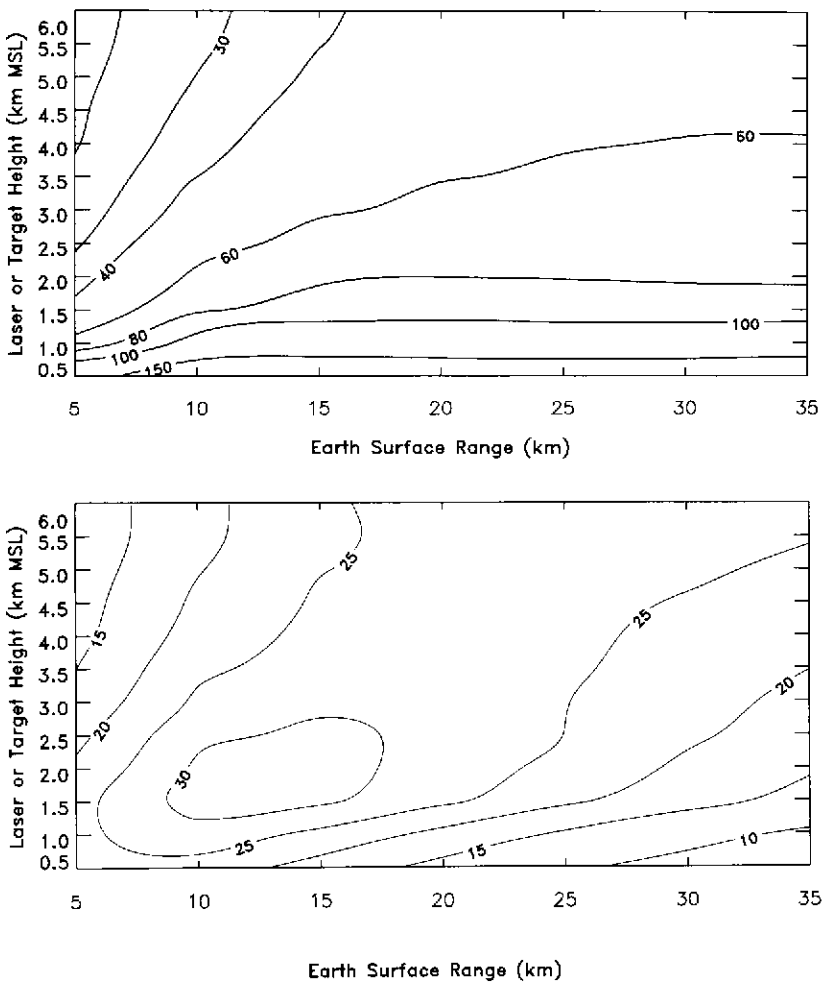

Fig. 5. Contour analyses of mean distortion number N_d for 360-deg (top) and 45-deg (bottom) azimuth as a function of upper-end altitude (kilometers MSL) and earth surface range (kilometers) for the Bahrain summer 1997 measurement campaign. The laser aperture radius is 50 cm, and the laser power is 10^5 W.

earth surface distances exceeding 7 km. However, when the target lies at a 45-deg azimuth angle (lower figure), the transverse component of flow is sufficiently large so that the largest values of N_d are less than 35 and confined to the shorter ranges. The shorter ranges in this case are less influenced by slew velocity. In the case of the larger azimuth angles $\geq$45 deg, uncompensated blooming effects may still be significant but phase compensation could be used to minimize atmospheric effects. The mean distortion number patterns observed in Fig. 5 generally apply for the other campaigns as analyzed according to azimuth angle.

5. Discussion of Results

Table 2 lists by thermosonde measurement campaign the range of distortion numbers and the average of distortion numbers for each azimuth angle over all altitudes and ranges.

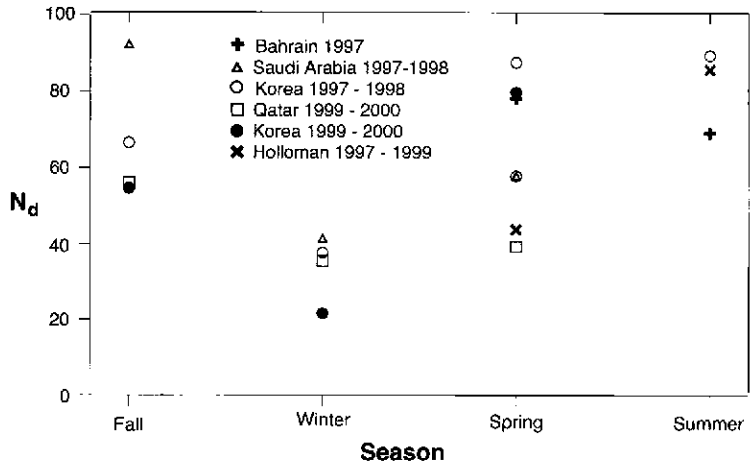

Fig. 6. Plots of mean distortion number by season for different measurement locations (360-deg azimuth).

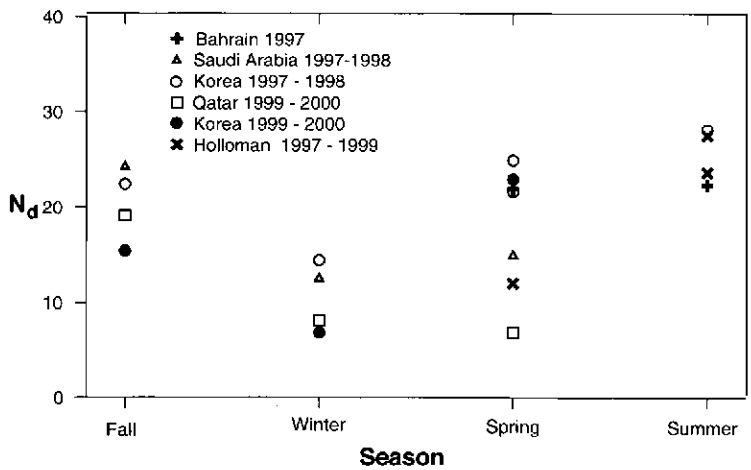

Fig. 7. Plots of mean distortion number by season for different measurement locations (45-deg azimuth).

In each column, the largest and smallest values of distortion number are highlighted in boldface and boldface italics, respectively. Figures 6–8 depict plots of the mean distortion numbers of Northern Hemisphere campaigns for all altitudes and ranges by season for each azimuth angle.

For azimuth angles of 360 deg, the typical range of mean N_d is from less than 10 to greater than 200. For 45 deg, the typical range of mean N_d is less than 10 to greater than 40. For 90 deg, the range of N_d is from less than 5 or 10 to greater than 30. Thus, the slew transverse flow component plays a very large role in modulating the typical range of distortion numbers encountered. It is also evident from Table 2 that for the Northern Hemisphere, the smallest values of distortion number tend to occur in winter and the largest values tend to occur in the spring or summer seasons. This is illustrated in Fig. 6, which is

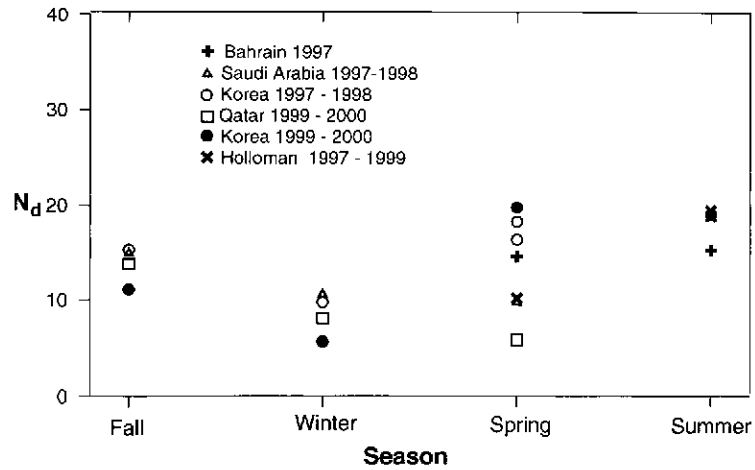

Fig. 8. Plots of mean distortion number by season for different measurement locations (90-deg azimuth).

a plot of mean distortion number by season and geographic location for the 360-deg target azimuth. Note that there tends to be a greater range of the mean values of distortion number during spring than in other seasons. This same behavior holds also for the azimuth angles of 45 and 90 deg, which are depicted in Figs. 7 and 8.

In Eq. (2), the distortion number is dependent on the absorption coefficient α. Considering that the major contribution to absorption at 1.315 μm is water vapor molecular line absorption for altitudes below 6 km, a measure of the path-integrated water vapor content should be helpful in inferring changes in the distortion number between seasons and locale. One measure is slant path precipitable water (SPW). This represents the depth of water resulting if all the water vapor along the laser path between the two ends were condensed. SPW is expressed as

$$\mathrm{SPW} = \int_0^S \frac{w\rho_d}{\rho_\ell}\,\mathrm{d}s \qquad \text{(cm)}, \tag{5}$$

where w is the water vapor mixing ratio, ρ_d is the density of dry air, and ρ_ℓ is the density of liquid water. SPW can be estimated using several methods. These include radiosonde measurements of humidity (e.g., Ref. 11) and the differential absorption lidar (DIAL) technique along the laser propagation path.[3] It can also be determined using passive remote sensing methods such as microwave radiometry[6] or refractive path delay of 1.2- and 1.6-GHz carrier signals between global positioning system and ground stations.[18]

Figure 9 is a plot of mean campaign distortion number N_d as a function of mean SPW for all measurement campaigns listed in Table 2. The 360-deg azimuth value for N_d was used in the comparison since this angle had the minimum contribution to path transverse flow from the air-to-ground slew. The mean values for a campaign include all air-to-ground paths used to construct Figs. 5–8. N_d generally increases with increasing SPW up to about 20 cm, where the N_d maximum value of approximately 100 is obtained using a second-order, least-squares fit. Leveling off is indicated when SPW exceeds 20 cm. The leveling may be a result of increased path extinction associated with the increased water vapor line absorption. The outlying mean value $N_d = 194$ is associated with the Holloman fall 1997

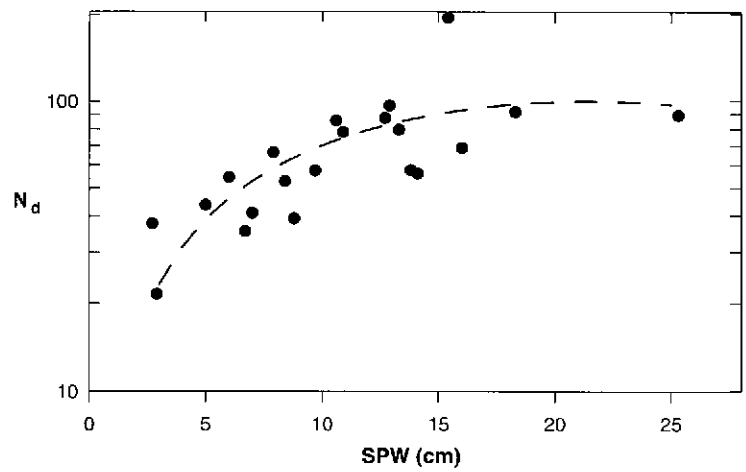

Fig. 9. Mean atmospheric distortion number vs. mean slant path precipitable water (centimeters) for 360-deg azimuthal heading for campaigns listed in Table 2. Each circle represents a campaign mean value. Dashed curve marks a second-order, least-squares fit.

campaign. The reason for such high magnitudes is probably the occurrence of very low wind speeds during this particular measurement period (Sept. 1997).

6. Summary and Conclusion

Values of the nondimensional atmospheric distortion number N_d for nonlinear refraction have been calculated for different locations and seasons using thermosonde measurements. The distortion number N_d allows inference of the degree of nonlinear refraction or thermal blooming associated with an atmospheric HEL path. For a CW laser with a Gaussian-shaped beam, the distortion number is a function of several variables including the HEL beam characteristics, atmospheric variables including temperature, moisture, pressure, and wind velocity and laser path characteristics including location or position and slew rate. The laser paths used in the calculations encompass a range of air-to-ground tactical scenarios for altitudes up to 6 km ASL. Scenario-dependent calculations are accomplished for different geographical regions and seasons using the Air Force Research Laboratory's global thermosonde database, the HITRAN molecular absorption line parameters database, and OPAC/GADS aerosol extinction models for the COIL wavelength of 1.315 μm. Subsonic beam transverse flow is assumed.

Our results, using fixed HEL parameters, exhibit a wide range of distortion number values depending on the particular path scenario and azimuth or aspect angle. This range is directly related to the path's location in the atmosphere and the transverse flow associated with its slew velocity. For the case of head-on azimuth, distortion number values can exceed 100 for air-to-ground paths exceeding 10 km in length and originating below 1.5 km AGL. The availability of accurate wind data is critical to this case's determination. For paths with the larger azimuth angle ($\geq$45 deg), typical values did not greatly exceed 40, while distortion values at the largest azimuth angle (90 deg) were even lower. Averages of the distortion number for all laser scenario paths by season and location were lowest in winter, while the

greatest range of distortion number values occurred during spring. It was observed that the average distortion number for all paths during a measurement campaign correlated with the average water vapor content found along the path. This correlation is primarily due to the large dependence of molecular absorption at 1.315 μm on water vapor or relative humidity.

Considerable uncertainty exists for these results; thus the term "estimate" is used in the title of this paper. This includes the inability to account for aerosol absorption and extinction properties as a function of the HEL irradiance magnitude by neglecting the ratio of aerosol vaporization energy to the aerosol energy conducted into the air, the uncertainty in aerosol extinction associated with the parameterization of aerosol optical properties and structure using weather and aerosol climatologies, and the consideration of only CW and not pulsed laser systems. Also, these results do not include scintillation effects due to refractive turbulence, which can have a large effect on the laser irradiance field, especially in the lower atmosphere regime investigated here. The results may prove helpful to future research efforts that seek quantification of atmospheric effects on HEL propagation. The same analysis approach, if proved worthy, could be applied to the larger set of global synoptic rawinsonde data for a more extensive analysis.

7. Acknowledgments

The authors acknowledge helpful comments from journal reviewers that improved the manuscript. This study was supported by the DOD High Energy Laser Joint Technology Office (HEL JTO).

References

[1]Born, M., and E. Wolf, *Principles of Optics*, Pergamon Press, Oxford (1980).

[2]Bradley, L.C., and J. Herrmann, Appl. Opt. **13**, 331 (1974).

[3]Dao, P., and A. Dentamaro, Proc. SPIE **5087**, 141 (2003).

[4]Fletcher, C. A. J., *Computational Galerkin Methods*, Springer-Verlag, New York (1984).

[5]Gebhardt, F.G., "Nonlinear Propagation: Thermal Blooming," in *The Infrared and Electro-Optical Systems Handbook, Vol.2, Atmospheric Propagation of Electromagnetic Radiation*, Environmental Research Institute of Michigan, Ann Arbor, pp. 287–313 (1993).

[6]Güldner, J., and D. Spänkuch, J. Atmos. Ocean. Tech. **18**, 925 (2001).

[7]Herrmann, J., and L.C. Bradley, "Numerical Calculation of Light Propagation," Report LTP-10, Lincoln Laboratory, Massachusetts Institute of Technology, Lexington, MA (1971).

[8]Hess, M., P. Koepke, and I. Schult, Bull. Am. Met. Soc. **79**, 831 (1998).

[9]Jursa, A.S. (ed.), *Handbook of Geophysics and the Space Environment*, Air Force Geophysics Laboratory, Hanscom Air Force Base, MA (1985).

[10]Koepke, P., M. Hess, I. Schult, and E.P. Shettle, "Global Aerosol Data Set," Report 243, Max-Planck Institüt für Meteorologie, Hamburg, Germany (1997).

[11]Kuo, Y.H., and Y.R. Guo, Month. Weath. Rev. **121**, 1215 (1993).

[12]McDermott, W.E., N.R. Pchelkin, D.J. Benard, and R.R. Bousek, Appl. Phys. Lett. **32**, 469 (1978).

[13]Rothman, L.S., R.R. Gamache, R.H. Tipping, C.P. Rinsland, M.A.H. Smith, D.C. Benner, V. Malathy Devi, J.-M. Flaud, C. Camy-Peyret, A. Perrin, A. Goldman, S.T. Massie, L.R. Brown, and R.A. Toth, J. Quant. Spectrosc. Radiat. Transfer **48**, 469 (1992).

[14]Sprangle, P., J. Peñano, and B. Hafizi, J. Directed Energy **2**, 71 (2006).

[15]Ulrich, P.B., "Numerical Methods in High Power Laser Propagation," in *Optical Propagation in the Atmosphere*, NATO AGARD Conf. Proc. 183, pp. 31-1–31-19 (1975).

[16]Wallace, J., and M. Camac, J. Opt. Soc. Am. **60**, 1587 (1970).

[17]Wallace, J., and J.Q. Lilly, J. Opt. Soc. Am. **64**, 1651 (1974).

[18]Ware, R., C. Alber, C. Rocken, and F. Solheim, Geophys. Res. Lett. **24**, 417 (1997).